Chapter 6
Soft Turn-Off Capacitively Coupled SSCBs for MVDC Applications

Fei Lu and Reza Kheirollahi

1 Introduction

Medium-voltage DC (MVDC) systems are growing worldwide [1]. Compared with alternative current (AC) counterparts, DC systems eliminate the need for frequency synchronization and reactive power compensation, facilitate using renewable energies, present potential advantages for integration of distributed generations and energy storage systems, and reduce the number of energy conversion stages [2, 3]. Besides, in recent years, a massive expansion of DC loads such as data centers and electric vehicle charge stations has been reported [4]. This highlights the significance of research in this field for both academia and industry.

However, the progress of MVDC systems faces technical limitations. Among many factors, circuit breakers are under early development [1, 5–7]. On one hand, due to the lack of zero crossing points in DC currents and the low inertia of DC systems, AC circuit breakers are not effective in interrupting large DC currents [8]. On the other hand, downsized versions of high-voltage DC (HVDC) circuit breakers do not lead to compact and efficient topologies [9]. Therefore, it suggests an urgent need to develop reliable, efficient, fast, and compact circuit breakers targeting MVDC applications.

Compared with mechanical and hybrid circuit breakers, SSCBs present remarkable advantages. They benefit from a fast response speed within microseconds, high compactness, and scalability [10–12]. Also, recent developments in wide bandgap semiconductor devices have resulted in more efficient circuit breakers as the result

F. Lu (✉) · R. Kheirollahi
Drexel University, Philadelphia, PA, USA
e-mail: fei.lu@drexel.edu; fl345@drexel.edu; reza.kheirollahi@drexel.edu

I. C. Kizilyalli et al. (eds.), *Direct Current Fault Protection*, Power Systems,
https://doi.org/10.1007/978-3-031-26572-3_6

of smaller on-state resistance and extended electrical ratings [13, 14]. In contrast, achieving high efficiency in SSCBs leads to an expensive design [13]. According to the survey conducted in [15], most of the design cost of an SSCB is related to solid-state switches. Therefore, the reliability of the solid-state switches in circuit breakers is of great importance.

Energy-absorbing components are inseparable from DC circuit breakers. DC systems include line inductors to slow down the rising rate of short circuit fault currents [16]. The corresponding inductive energy needs to be dissipated during DC current breaking. However, solid-state switches have a limited energy dissipation capability [17]. To overcome this difficulty, energy absorption components are employed. Metal oxide varistors (MOVs), paralleled MOVs, MOV and resistor-capacitor (MOV-RC), and MOV and resistor-capacitor-diode (MOV-RCD) snubbers are commonly used in conjunction with solid-state switches [14].

Passive snubbers have limitations in SSCBs. MOV-based snubbers clamp voltage oscillations well, but they bring extremely high dv/dt across the main switch. MOV-RC and MOV-RCD snubbers overcome this problem as snubber capacitance helps effectively during the transient; MOV-RCD has better current capability compared with the RC snubbers; however, they suffer from a conflict between the response speed and power shock reduction during DC current interruption [18]. That is, increasing the snubber capacitance decreases the power shock on the solid-state switches, but it elongates the reaction time interval in the breakers. The situation is worsened when ultrafast SSCBs aim to be optimally coordinated in DC systems [19].

This chapter deals with the application of auxiliary active injection circuits in eliminating power shock on solid-state switches in SSCBs. Active injection circuits have been reported in mechanical and hybrid breakers to alleviate the arcing problem in mechanical disconnectors during DC current interruption [20–22]. In mechanical breakers, the countercurrent pulse is generated by a resonant LC circuit, and it is controlled by an injection switch. The injection capacitor in the auxiliary branch can be charged by an external charger [22] or through the DC system itself [23]. The former gives the flexibility of adjusting the injected pulse current's amplitude and duration, while the latter benefits from simplicity. The injection capacitor and inductor are chosen regarding the fastness of the main switch S_{m}, the maximum fault current aimed to be interrupted in the system, the maximum voltage value on the injection capacitor, and the power density limitation of the targeted design.

The capacitive coupling interface is also introduced in this chapter, where it helps to enhance reliability in active injection-based breakers. In DC breakers where the auxiliary branch is directly connected to the main branch, they are prone to short circuit faults in the auxiliary injection circuits. This puts the reliability of DC systems at serious risk. To avoid this issue, capacitive couplers are introduced which act as the interface between the main and auxiliary branches and block short circuit fault currents. The operation of MVDC SSCBs based on a capacitive coupling interface will be demonstrated throughout the chapter.

2 Soft Turn-Off Operation in SSCBs

Even though solid-state switches in DC breakers undergo a limited number of switching, they experience large dv/dt and di/dt values. These result in high gate voltage oscillations leading to device failure or false turn-on operation during DC current interruption. MOV-RCD snubber circuits are considerably effective in mitigating the mentioned phenomenon; however, they are not able to fully solve the problem [24, 25].

High power shock on solid-state switches during the dc current interruption is another critical reliability issue. In SSCBs, solid-state switches are responsible for interrupting large DC currents. In this case, depending on fault currents amplitude and the snubber circuits, a relatively large transient power may appear on the solid-state switches [24]. Accordingly, high transient energy produces in the switches during a very short period [18].

This transient energy could be the source of two major separate failures including gate degradation and thermal runaway [26]. These two failures are the result of the fast growth rate of the temperature inside the device. The temperature dynamic and its growth rate are proportional to the transient power and energy in which the device is subjected to. Degradation and thermal runaway temperatures are two distinct boundaries in solid-state switches. The degradation of the gate structure occurs when the surface is exposed to degradation temperature for a sufficient time. This results in partially or entirely losing current conduction capability. In case the temperature reaches the thermal runaway boundary, the drain current increases exponentially followed by a permanent device failure.

Gate voltage oscillations and transient power are current-dependent. Meaning that reducing the current amplitude in solid-state switches during DC current interruption helps to mitigate the pointed challenges. The soft turn-off is a promising solution in this matter [22, 24], which will be elaborated in the following.

Soft turn-off operation refers to the situation in which the DC current in the switch is forced to zero during dc current breaking. To achieve this, active injection circuits with precharge injection capacitors are utilized. The general structure of the presented concept is shown in Fig. 6.1a. The breaker includes three branches connected in parallel: main branch, auxiliary branch, and energy-absorbing branch, illustrated in the following.

The critical current and voltage waveforms of the soft turn-off breaker are shown in Fig. 6.1b. In normal operating mode, the main branch conducts the load current through the main switch S_{m}, and current in the auxiliary and energy-absorbing branch is zero. It is assumed that a short circuit fault occurs at $t = t_0$, and the system current begins to increase. The current interruption process includes three main stages: the current reaction process, soft turn-off operation, and energy absorbing stage.

During the reaction time interval ($t_1 \leq t < t_2$), a countercurrent pulse is created by the auxiliary branch, and it is injected into the main branch to cancel the fault current in the main switch. Next, at $t = t_2$, when the current in the main switch S_{m}

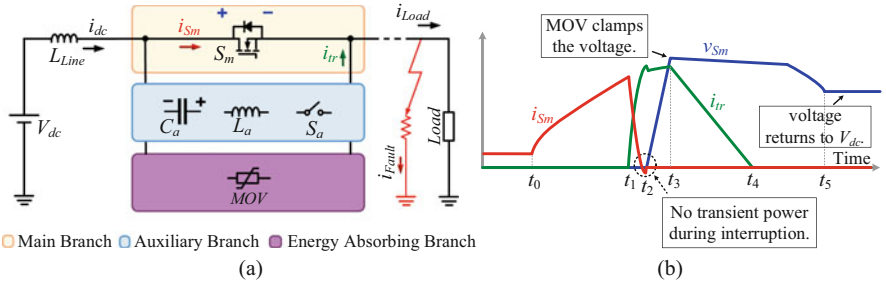

Fig. 6.1 Soft turn-off operation [22]. (**a**) The general structure of active current injection-based SSCBs is shown; the main branch includes solid-state switches; the auxiliary branch consists of injection components, and the energy-absorbing branch involves MOVs (**b**) Corresponding critical current and voltage waveforms (labeled in Fig. 6.1a) are represented

reduces to zero, S_m is triggered to be OFF. Then, the commutated fault current in the auxiliary branch is interrupted, forcing the fault current to the energy-absorbing branch ($t_3 \leq t < t_5$). Finally, the energy-absorbing elements dissipate the stored inductive energy of the line inductor.

The operation of the breaker shown in Fig. 6.1 reveals the soft turn-off during the DC current interruption. First, at the time of turning off the main switch, the current in the main switch is almost zero, which helps to mitigate the gate voltage oscillations. Also, as labeled in Fig. 6.1b, when the voltage across the solid-state switch begins rising, the current in the switch is zero, meaning zero power shock in the solid-state switch. All of these features are effective in enhancing the reliability of the breaker and extending its lifetime [24].

There are two kinds of modularity in the soft turn-off SSCBs. Regarding Fig. 6.2a, multiple solid-state switches can be connected in parallel to achieve higher efficiency and current interruption capability [14]. In this case, to achieve a soft turn-off operation, each solid-state switch is accompanied by its auxiliary and energy storage branches. In addition to simplicity during the design procedure, this kind of modularity results in current scalability, which is highly useful for the future development of DC systems. Also, it is highly effective in addressing any possible glitch between digital signals received by multiple solid-state switches in the main branch. In other words, if one of the switches in the main branch turns off sooner, the provided modularity prevents any damage to other switches due to resulted uneven current distribution.

Figure 6.2b indicates the second type of modularity, where multiple active injection auxiliary branches are connected in parallel to the main branch [22]. The goal is to obtain injection countercurrent pulses with different amplitudes for fault currents under different fault resistances. Each auxiliary branch could involve a unique injection inductor, resulting in a unique injection countercurrent pulse. Modularity can be achieved by activating different combinations of auxiliary branches during DC current interruption. Each auxiliary branch may include its precharge injection capacitor, or all the auxiliary branches can share one injection

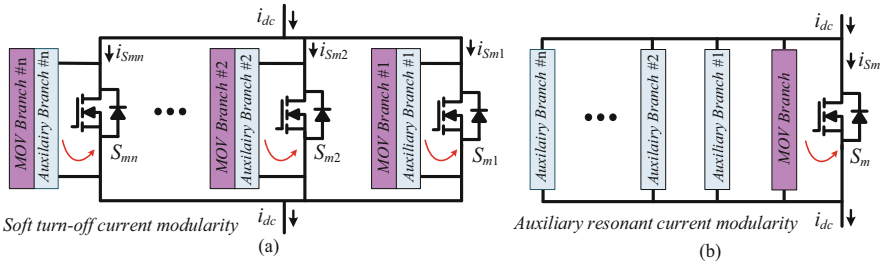

Fig. 6.2 Implementing modularity in soft turn-off SSCBs. (**a**) Each solid-state switch has its auxiliary and MOV branches. (**b**) Modularity in this topology can be achieved by generating countercurrent pulses with adjustable amplitudes and durations

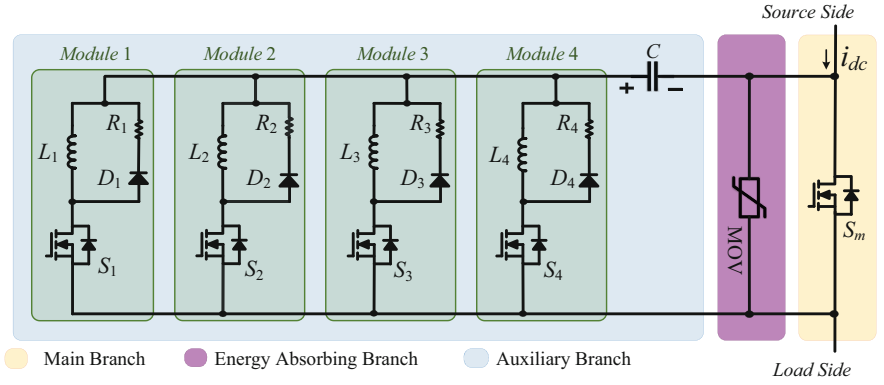

Fig. 6.3 Modular active injection circuits in a soft turn-off SSCB corresponding to Fig. 6.2b [22]. The auxiliary branch includes one injection capacitor; however, multiple injection inductors are connected in parallel. The value of injection inductors is optimized to achieve adjustable pulse currents

capacitor as shown in Fig. 6.3 [22]. For both cases, the SSCB only consists of one MOV branch directly connected in parallel to the main branch.

On the other hand, DC circuit breakers with active injection circuits shown in Fig. 6.1 are prone to short circuits in the auxiliary branch. This practical issue could reduce the reliability of the implemented protection systems and result in safety challenges. Figure 6.4 shows two general structures of DC circuit breakers with auxiliary circuits in DC systems. In Fig. 6.4a, the precharge injection capacitor is fully charged through an external charger; while in the topology of Fig. 6.4b, the injection capacitor is charged by the DC system itself controlled by a charging switch.

In both structures of Fig. 6.4, the potential failures are shown [27]. In Fig. 6.4a, the short circuit failure path creates its way through the injection inductor L_a, the injection switch S_a, and the external charger V_{Ch}-S_{Ch}. In such a short circuit failure, the circuit breaker is bypassed, leaving the DC system without protection. In the

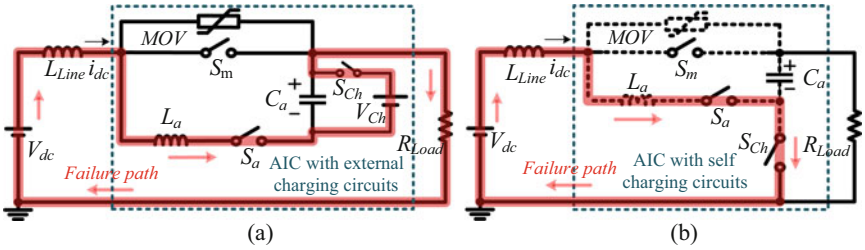

Fig. 6.4 Potential short circuit failures in active injection circuit-based circuit breakers [27]. (**a**) A short circuit may occur through the external charging converter, bypassing the circuit breaker and leaving the DC system without any protection. (**b**) Short circuit failure may occur through the injection switch S_{ch}, resulting in a short circuit in the DC link

second scenario of Fig. 6.4b, the failure path leads to a short circuit close to the DC source; the fault is created through the injection inductor L_a, the injection switch S_a, and the charging switch S_{Ch}. Although a residual current mechanical disconnector can separate the circuit breakers from the DC source during the OFF-state, it is not practical when multiple SSCBs are in the DC systems [28, 29]. Therefore, solving the problem inside the circuit breakers is more effective.

3 Capacitively Coupled Soft Turn-Off SSCBs

A capacitive couple-based interface is a promising solution to prevent the potential failures described in Fig. 6.4. The general topology is shown in Fig. 6.5a [27]. The auxiliary branch is connected to the main branch through two coupling capacitors. The couplers allow the transient pulse currents during DC current interruption, but they prevent short circuit faults in the case of any failure. The coupling capacitance is in the range of hundreds of nano-Farad, which can be easily built using couplers with enough airgap for the sake of voltage isolation. As the capacitance is low, it does not reduce the power density of the final design.

Regarding Fig. 6.5, a few points can be highlighted below:

1. As coupling capacitors are in the range of hundreds of nano-Farad, the injected pulse current during DC current interruption should be short with sufficient flat-top profile (Δt_β in Fig. 6.5b) to achieve soft turn-off operation.
2. The auxiliary branch is completely isolated from the DC power system; in this case, an external charger is used to charge the injection capacitor C_a in the auxiliary branch.
3. When the main switch S_m is ON, the voltage across the coupling capacitors is almost zero. During the turn-off process, coupling capacitors share the DC bus voltage. Also, overshoot voltages across the couplers can be clamped as will be further described in the section.

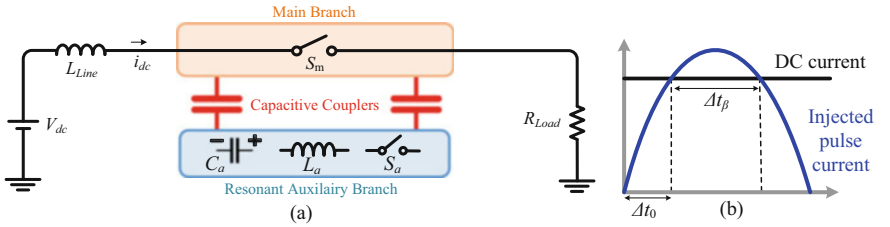

Fig. 6.5 Capacitively coupled current commutation [27]. (**a**) A capacitive couple-based interface between the main branch and the auxiliary branch is shown. Coupling capacitors allow pulse current to flow through between two branches, but they block the flowing of short circuit fault currents. (**b**) The emulated injected pulse current and the DC fault current are shown in (**b**); Δt_β is required to achieve a soft turn-off operation; Δt_0 should be minimized to optimize coupling capacitors

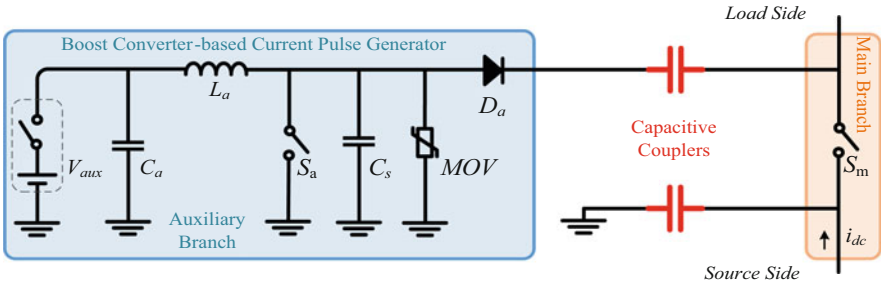

Fig. 6.6 Boost converter-based current pulse generator is represented [30]. The current pulse generator is designed using the working principle of the Boost converters

4. A well-defined digital communication is required between the main and auxiliary branches during DC current interruption.
5. Both modular topologies illustrated in Fig. 6.2 can be applied to the capacitively coupled SSCBs.
6. Energy-absorbing elements can be directly connected in parallel to the main branch, and it does not interfere with the operation of the auxiliary branch and the capacitive couplers.

With respect to Fig. 6.5a, the auxiliary active injection branch should generate a pulse current with a short duration to optimize the coupling capacitors. That is, Δt_β of Fig. 6.5b aims to be decreased as much as possible, which helps to reduce charge currents flowing through the coupling capacitors. To achieve this goal, the Boost converter-based current pulse generator of Fig. 6.6 is highly applicable [30].

The current pulse generator mainly includes an auxiliary low voltage DC source V_{aux}, an injection precharge capacitor C_{a}, an injection inductor L_{a}, an injection controlling switch S_{a}, a snubber capacitor C_{s}, an MOV element for protecting the injection switch, and an output diode D_{a}. The auxiliary branch is connected in

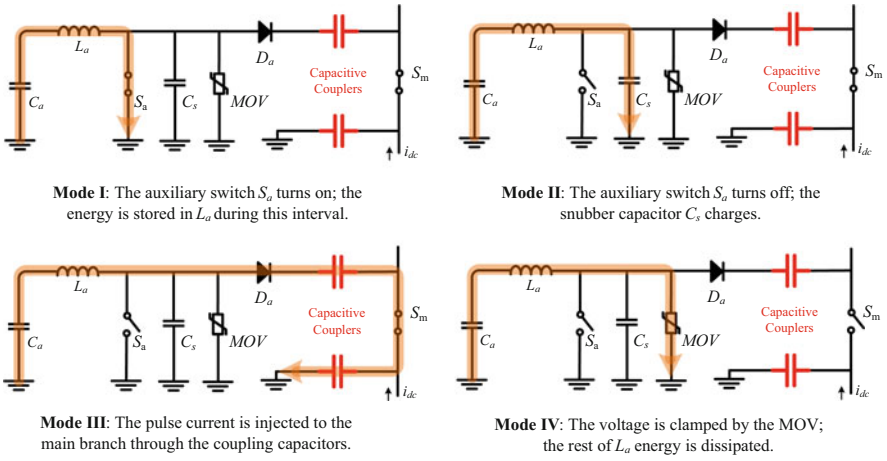

Mode I: The auxiliary switch S_a turns on; the energy is stored in L_a during this interval.

Mode II: The auxiliary switch S_a turns off; the snubber capacitor C_s charges.

Mode III: The pulse current is injected to the main branch through the coupling capacitors.

Mode IV: The voltage is clamped by the MOV; the rest of L_a energy is dissipated.

Fig. 6.7 The operating modes of the Boost converter-based current pulse generator are represented [30]. It is assumed that the injection capacitor C_a is charged by the auxiliary source V_{aux}, and V_{aux} is not involved in the presented analysis

parallel to the main branch through the capacitor couplers. The main branch consists of MOSFET switches whose body diodes help achieve soft turn-off operation.

Figure 6.7 indicates the operating modes of the Boost converter-based current pulse generator in injecting a countercurrent pulse current to the main switch S_m. The operation is explained in the following.

Mode I The auxiliary switch S_a turns on, and the energy stored in the precharge injection capacitor C_a is transferred to the injection inductor L_a. The inductor current begins to increase whose slope depends on the pre-charge voltage on the injection capacitor V_{aux}, the injection capacitance C_a, and the injection inductance L_a. During this mode, no current flows through diode D_a and capacitive couplers. Also, as the injection switch S_a is ON, the voltage across the snubber capacitor C_s, the MOV, and coupling capacitors remains zero.

Mode II The amplitude of the injection inductor current reaches a threshold value specified in the SSCB; then, the control algorithm triggers the injection switch S_a to be OFF. In this case, the snubber capacitor C_s, connected in parallel to S_a, starts charging. The value of C_a is chosen optimally to protect S_a from high dv/dt during the turn-off process. The voltage across C_a continues increasing; the current in the injecting diode D_a is still zero.

Mode III The voltage across the snubber capacitor C_s reaches the auxiliary voltage V_{aux}. The injection diode D_a turns ON, where it begins to conduct the countercurrent pulse and inject it to the main branch through the capacitive couplers. Simultaneously, the current in the main switch S_m reduces to zero, obtaining a current zero-crossing point in the main switch. As the current approaches zero in S_m, the main branch's control board turns S_m off, meaning a soft turn-off operation,

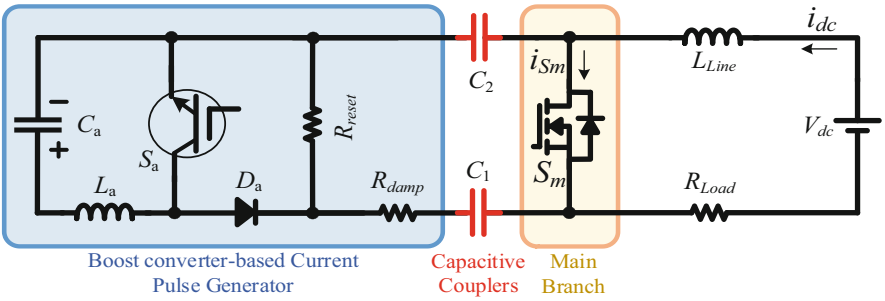

Fig. 6.8 Capacitive couple-based SSCB is shown in a medium voltage DC system with the line inductor L_{Line} and the resistive load R_{Load} [27]. The Boost converter-based current pulse generator is connected to the main branch through coupling capacitors C_1 and C_2

e.g., Fig. 6.1b. It is noted that the body diodes of the main switch S_{m} are effective, highlighted in the next section.

Mode IV As the pulse current flows through the capacitive couplers, the coupler's voltage rises. As the voltage reaches the clamping voltage of the snubber MOV, the MOV switches to the clamping mode. The MOV's resistance reduces significantly and conducts the tail of the injection inductor current L_{a}. In this case, the current in the injection diode D_{a} and the coupling capacitors reduces to zero. The MOV continues in the conduction mode till it absorbs all the energy of the injection inductor L_{a}. Finally, the MOV returns to the leakage current mode and blocks the auxiliary voltage V_{aux}.

The design procedure of the current pulse generator has been well described in [30]. The primary aim is to obtain a countercurrent pulse with sufficient amplitude and profile to implement a reliable soft turn-off during DC current interruption. The next design objective is minimizing the capacitance of the couplers, as it helps to achieve a compact and low-cost design. Therefore, the auxiliary source voltage V_{aux}, the injection capacitor C_{a}, the injection inductor L_{a}, and the clamping voltage of the snubber MOV along with all the parasitic components are included in the design procedure.

Regarding the soft turn-off technique, the capacitive couple-based interface, and the Boost converter-based pulse current generator, an MVDC soft turn-off SSCB with the capacitive couple interface is developed and analyzed. Figure 6.8 indicates the capacitively coupled MVDC SSCB [27]. The dc bus voltage is V_{dc}, L_{Line} emulates the line inductor, and the load is assumed to be resistive R_{Load}. The main branch is constructed from SiC power MOSFET modules. The auxiliary branch follows the same topology as the current pulse generator in Fig. 6.6. Capacitive couplers are labeled as C_1 and C_2 whose values are assumed to be the same, meaning $C_1 = C_2 = C$.

As indicated in Fig. 6.8, the current pulse generator also includes the couplers reset resistor R_{reset} and the damping resistor R_{damp}. The couplers' reset resistor

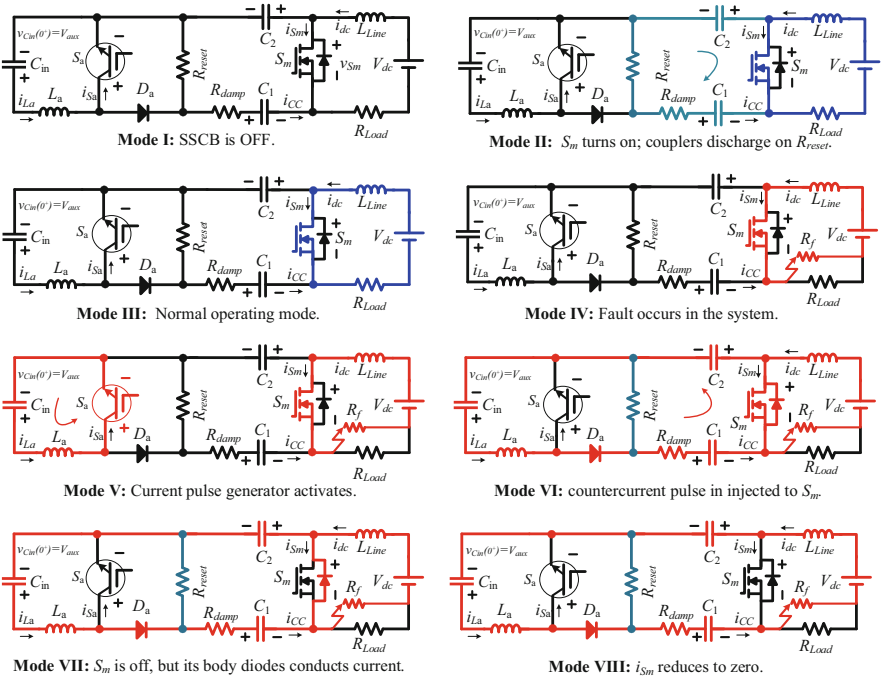

Fig. 6.9 The operating modes of the capacitive couple-based SSCB are shown [27]. The circuit breaker is in a DC system with the line inductor L_{Line} and the load R_{Load}. Modes II and III indicate the closing process and couplers reset mode. Also, a short circuit fault is emulated by R_{f}, where it starts from mode IV. The circuit breaker reacts to fault in mode V

is used to discharge the capacitive couplers when the main switch S_{m} turns on, but small values of R_{reset} result in leakage currents during the breaker OFF-state. Therefore, a tradeoff should be made in selecting R_{reset}. Also, the damping resistor R_{damp} damps the ringing flat-top of the injected countercurrent pulse, but large values of R_{damp} lead to a small Δt_{β} shown in Fig. 6.5b.

The operating modes of the capacitively coupled soft turn-off SSCB are shown in Fig. 6.9, where the closing process, normal operating mode, and fault current interruption are indicated. Also, the corresponding critical electrical waveforms of Fig. 6.9 are displayed in Fig. 6.10. Regarding Figs. 6.9 and 6.10, the operation of the breaker is explained below.

During mode I (before t_0), the circuit breaker is OFF. The DC bus voltage places on the main branch $v_{\text{Sm}} = V_{\text{dc}}$. In the auxiliary branch, the injection capacitor C_{a} charges to V_{aux} using an auxiliary voltage source $V_{\text{Cin}} = V_{\text{aux}}$. As the current in the injection inductor L_{a} is zero, the injection switch S_{a} holds the same V_{aux} voltage, meaning $v_{\text{Sa}} = V_{\text{aux}}$. Each capacitive coupler holds half of $V_{\text{aux}} + V_{\text{dc}}$. It is noted that both coupling capacitors are assumed to be the same; in this case, $v_{C1} = v_{C2}$.

The circuit breaker turns on during modes II and III ($t_0 \leq t < t_1$) and undergoes its closing stage and capacitive couplers' reset process. S_{m} turns on at $t = t_0$ and

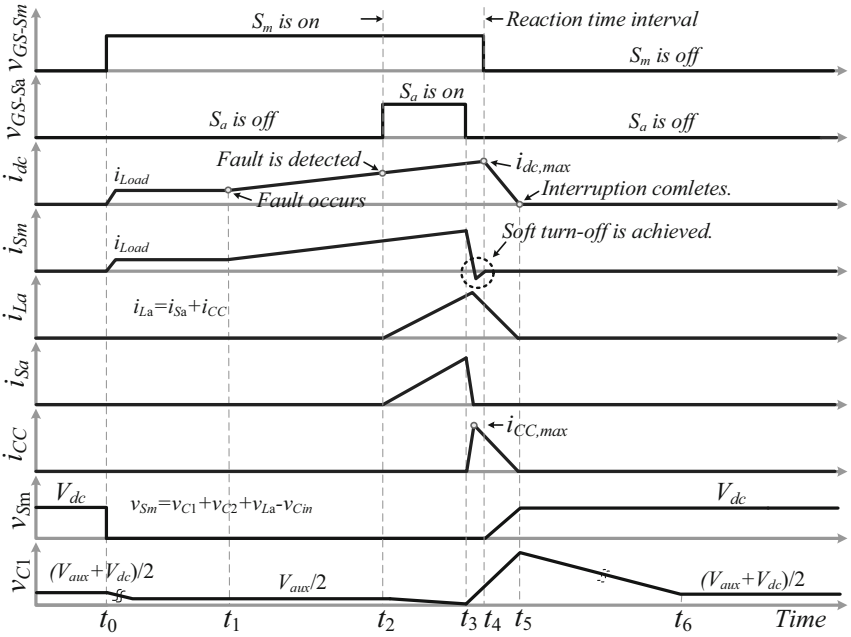

Fig. 6.10 The critical electrical waveforms of the capacitive couple-based SSCB are shown [27]. The intervals consist of the OFF-state (mode I before t_0), closing stage (mode II at $t = t_0$), couplers reset mode (mode II during $t_0 < t < t_1$), normal operating mode (mode III during $t_0 < t < t_1$), fault occurrence (mode IV during $t_1 \leq t < t_2$), and fault current interruption ($t_2 \leq t < t_6$) are shown

conducts the load current. The capacitive couplers begin discharging on the reset resistor R_{reset}, where their voltage finally reaches $v_{C1} = v_{C2} = V_{\text{aux}}/2$. The current in the auxiliary branch remains zero. There is a leakage current in resistor R_{reset}, but it is negligible.

A short circuit fault with the fault resistance R_{f} occurs at $t = t_1$ during mode IV. The circuit breaker reacts to the fault during mode V by turning on the injection switch S_{a} ($t_2 < t < t_3$). Consequently, the pulse current in the injection inductor L_{a} increases. As shown in mode VI, at $t = t_3$, S_{a} turns off, and the current of the injection inductor L_{a} flows through the capacitive couplers as also described in Fig. 6.7.

In mode VII, at $t = t_4$, the main switch S_{m} current reduces to zero, and S_{m} is triggered to be OFF. A soft turn-off operation is achieved, where S_{m} turns off under zero power shock. During mode VIII ($t_4 < t < t_5$), the fault current commutates to the auxiliary branch, and it finally reduces to zero. Also, the remaining inductive energy of the injection inductor L_{a} is dissipated in the snubber MOV (refer to Fig. 6.7). The interruption completes, and the circuit breaker goes back to mode I. The voltage on S_{m} stabilizes on V_{dc}, and the voltage on each coupler is $(V_{\text{aux}} + V_{\text{dc}})/2$.

4 Experimental Study of Capacitively Coupled-Based SSCBs in MVDC Systems

To further analyze the proposed capacitively coupled soft turn-off SSCB, it is experimentally studied [30, 31]. Figure 6.11 shows the experimental setup. The SSCB is shown in Fig. 6.11. In the main branch, 12 CAB-450M12XM3 SiC MOSFET power modules are connected in a 4 × 3 matrix. MOV-RCD snubber circuits include MOV V661HA40, the snubber diode C4D20120, and 100 Ω and 200 nF as the snubber resistor and capacitor, respectively. The main branch gate drivers are supplied by an inductive wireless power transfer system to obtain voltage isolation between four layers. The main branch is controlled by a TMS320F28335 DSP from TI.

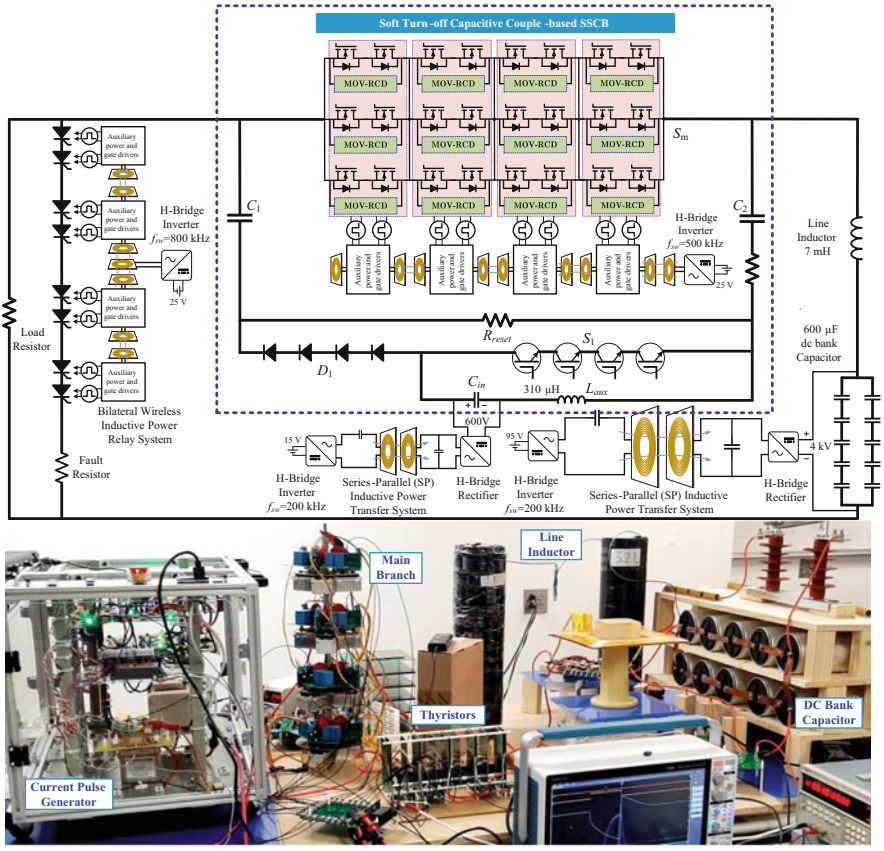

Fig. 6.11 4 kV/100 A DC short fault current interruption setup [31]. The system involves a 600 μF DC link capacitor charged to 4 kV using an inductive wireless capacitor charger. The line inductor is 7 mH; the load resistance is set to 285 Ω. Thyristor switches are used to emulate a short circuit fault current. The schematic of the soft turn-off capacitive couple-based SSCB is highlighted, where main branch switches are constructed from 12 SiC power modules in a 3 × 4 matrix

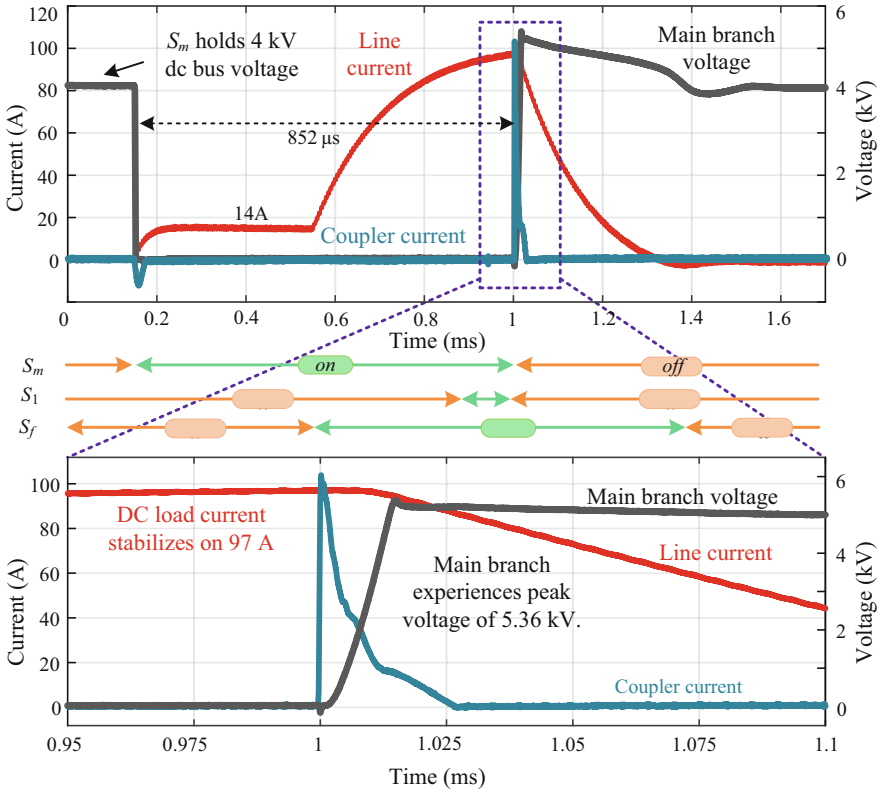

Fig. 6.12 Experimental results of the soft turn-off capacitive couple-based SSCB [31]. The main branch voltage, line current, and capacitive couple current waveforms are represented

Two 280 nF/10 kV film capacitors are used as the coupling interface between the main and auxiliary branches. In the auxiliary branch, two 5SNG-0300Q170300 IGBT power modules are used for the injection switch S_a. The injection inductor is $L_a = 314$ µH; the injection capacitor $C_a = 200$ µF, where its voltage is kept at 600 V using a series-parallel inductive wireless power transfer converter. The injection diodes are C4D20120, and the R_{reset} and R_{damp} resistors are 3 kΩ and 15 Ω, respectively. The breaker is tested in a 4 kV DC system, where the line inductor is 7 mH and the resistive load is 285 Ω. To emulate a short circuit fault, four MCNA650P2200CA thyristors are connected in series, where a bilateral wireless power relay system is used to trigger the thyristors reliably.

Figure 6.12 shows the experimental results. The line current, capacitive coupler currents, and the main branch voltage are indicated. In steady-state, the circuit breaker supplies 14 A load current. A short circuit fault is created at $t = 550$ µs through the thyristor switches. The breaker interrupts the fault current within 77 µs, where the peak of system current reaches 97 A and S_m experiences 5.36 kV overshoot voltage.

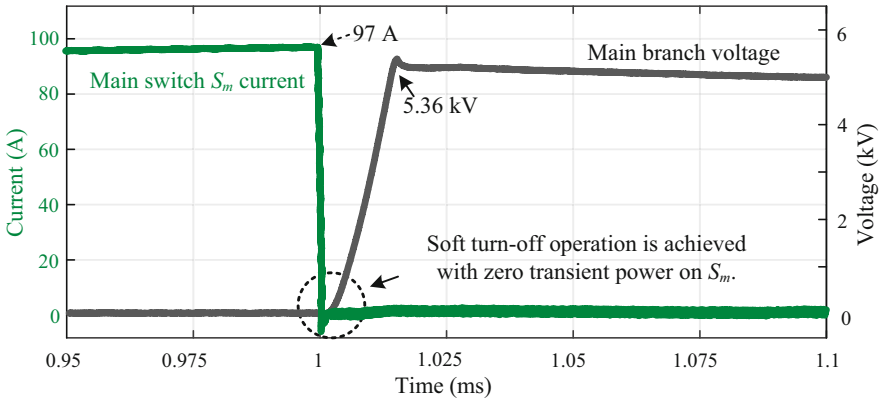

Fig. 6.13 Experimental results of the soft turn-off capacitive couple-based breaker. The main branch voltage and the main switch current waveforms are shown. As indicated, the main switch S_m turns off under zero power shock

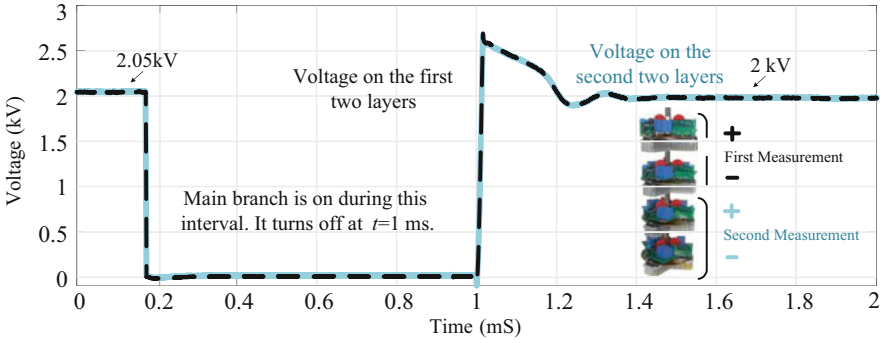

Fig. 6.14 Experimental results of the soft turn-off capacitive couple-based breaker [31]. The voltage balance between different layers of the main branch is shown. The voltage measurements indicate a voltage balance between the top two layers and the bottom two layers

Figure 6.13 reveals one of the promising advantages of the soft turn-off SSCB based on a capacitively coupled interface. The main switch current and the main branch voltage waveforms are displayed in Fig. 6.13. According to the operation of the capacitive couple-based SSCB, the main switch S_m turns off when the current in S_m reduces to zero. That is, the main switch voltage rises when there is no current in S_m, leading to a zero transient power on the main switch. This point has been highlighted in Fig. 6.13. The achieved zero power shock in the main switch S_m obtains a safe operation, improves its current interruption capability, and helps to enhance reliability.

Furthermore, Fig. 6.14 shows the transient voltage balance between the top and bottom layers during DC current interruption, which verifies the effectiveness of the

implemented symmetrical and efficient structure in the main branch. As is clear in Fig. 6.14, the voltage of the top two layers and the bottom two layers are evenly balanced during the transient and steady-state operation.

5 Conclusions

Applying transient current commutation to DC SSCBs achieves a soft turn-off operation during current interruption. For soft turn-off SSCBs, in the main branch, the voltage and current waveforms of the main switch have no overlaps during the turn-off process, leading to zero transient power and energy. Also, reducing the main switch current to zero mitigates the gate's voltage oscillations, resulting in a higher degree of reliability. When the main switch experiences a high change in its drain-source voltage, its gate voltage has already stabilized at zero or negative values, which reduces the possibility of a false turn-off. All these advantages improve the reliability of the SSCBs and extend the lifetime in the long term. Meanwhile, the active injection branch is fast and compact under modularity and scalability.

A capacitive couple-based interface between the main and auxiliary branches enhances the reliability of the DC system under operation. It prevents short circuits in the DC link close to the upstream breakers. In the meantime, a Boost converter-based current pulse generator allows transient current commutation through capacitive couplers. The current pulse generator works with a low-voltage auxiliary source, its generated pulse current is adjustable in terms of amplitude and duration, and it communicates synchronously with the main branch in a reliable manner. As the injected pulse current is short, the coupling capacitors' values are small, resulting in a compact design. The capacitively coupled soft turn-off MVDC SSCBs are a promising solution for implementing a robust protection system in MVDC power networks.

References

1. CIGRE, Medium voltage direct current (MVDC) grid feasibility study. Technical Brochure 793, WG C6.31 (2020)
2. S. Zheng, R. Kheirollahi, J. Pan, L. Xue, J. Wang, F. Lu, DC circuit breakers: A technology development status survey. IEEE Trans. Smart Grid **13**, 3915–3928 (2021). https://doi.org/10.1109/TSG.2021.3123538
3. F. Ornelas-Tellez, J. J. Rico-Melgoza, E. Espinosa-Juarez, E. N. Sanchez, Optimal and robust control in DC microgrids. IEEE Trans. Smart Grid **9**(6), 5543–5553 (2018)
4. K. Sun, H. Xiao, J. Pan, Y. Liu, A station-hybrid HVDC system structure and control strategies for cross-seam power transmission. IEEE Trans. Power Syst. **36**(1), 379–388 (2021)
5. X. Xu, W. Chen, C. Liu, R. Sun, Z. Li, B. Zhang, An efficient and reliable SSCB based on mixture device. IEEE Trans. Power Electron. **36**(9), 9767–9771 (2021). https://doi.org/10.1109/TPEL.2021.3067316

6. Z. J. Shen, Y. Zhou, R. Na, T. Cooper, M. A. Ashi, T. Wong, A series-type hybrid circuit breaker concept for ultrafast DC fault protection. IEEE Trans. Power Electron. **37**(6), 6275–6279 (2022)
7. R. Kheirollahi, S. Zhao, H. Zhang, F. Lu, Fault current bypass-based DC SSCB using TIM-pack switch. IEEE Trans. Ind. Electron. **70**, 4300–4304 (2022). https://doi.org/10.1109/TIE.2022.3174304
8. C.M. Franck, HVDC circuit breakers: A review identifying future research needs. IEEE Trans. Power Deliv. **26**(2), 998–1007 (2011)
9. G.F. Reed, B.M. Grainger, A.R. Sparacino, Z. Mao, Ship to grid: Medium-voltage DC concepts in theory and practice. IEEE Power Energy Mag. **10**(6), 70–79 (2012). https://doi.org/10.1109/MPE.2012.2212613
10. Z.J. Shen, Ultrafast SSCBs: Protecting converter-based AC and DC microgrids against short circuit faults. IEEE Electrif. Mag. **4**(2), 72–70 (2016). https://doi.org/10.1109/MELE.2016.2544058
11. R. Kheirollahi, S. Zhao, F. Lu, Fault current bypass-based LVDC SSCBs. IEEE Trans. Power Electron. **37**(1), 7–13 (2022)
12. D. Marroquí, J. M. Blanes, A. Garrigós, R. Gutiérrez, Self-powered 380 V DC SiC SSCB and fault current limiter. IEEE Trans. Power Electron. **34**(10), 9600–9608 (2019)
13. R. Rodrigues, Y. Du, A. Antoniazzi, P. Cairoli, A review of SSCBs. IEEE Trans. Power Electron. **36**(1), 364–377 (2021)
14. S. Zhao, R. Kheirollahi, Y. Wang, H. Zhang, F. Lu, Implementing symmetrical structure in MOV-RCD snubber-based DC SSCBs. IEEE Trans. Power Electron. **37**(5), 6051–6061 (2022). https://doi.org/10.1109/TPEL.2021.3133113
15. R. Kheirollahi, X. Zan, S. Zhao, Y. Wang, H. Zhang, X. Lu, A.T. Avestruz, F. Lu, A trade-off between cost and efficiency in SSCBs, in 2022 IEEE Energy Conversion Congress and Exposition, Detroit, Michigan, October 2022
16. J. Hafner, B. Jacobson, *Proactive Hybrid HVDC Breakers-A Key Innovation for Reliable HVDC Grid* (CIGRE, Bologna, 2011)
17. Z.J. Shen, Z. Miao, A.M. Roshandeh, SSCBs for DC microgrids: Current status and future trends, in Proceedings of IEEE 1st International Conference DC Microgrids, Atlanta, GA, USA (2015), pp. 228–233
18. S. Zhao, R. Kheirollahi, Y. Wang, H. Zhang, F. Lu, Investigation of limitations in passive voltage clamping-based solid-state DC circuit breakers. IEEE Open J. Power Electron. **3**, 209–221 (2022). https://doi.org/10.1109/OJPEL.2022.3163072
19. L. Qi, P. Cairoli, Z. Pan, C. Tschida, Z. Wang, V. R. Ramanan, L. Raciti, A. Antoniazzi, SSCB protection for dc shipboard power systems: Breaker design, protection scheme, validation testing. IEEE Trans. Ind. Appl. **56**(2), 952–960 (2020)
20. X. Pei, O. Cwikowski, D. S. Vilchis-odriguez, M. Barnes, A. C. Smith, R. Shuttleworth, A review of technologies for MVDC circuit breakers, in IECON 2016 – 42nd Annual Conference of the IEEE Industrial Electronics Society (2016), pp. 3799–3805, https://doi.org/10.1109/IECON.2016.7793492
21. Y. Zhou, Y. Feng, N. Shatalov, R. Na, Z. J. Shen, An ultraefficient dc hybrid circuit breaker architecture based on transient commutation current injection. IEEE J. Emerg. Sel. Top. Power Electron. **9**(3), 2500–2509 (2021)
22. R. Kheirollahi, H. Zhang, S. Zhao, J. Wang, F. Lu, Ultrafast SSCB with a modular active injection circuit. IEEE J. Emerg. Sel. Top. Ind. Electron. **3**, 733–743 (2022). https://doi.org/10.1109/JESTIE.2021.3087952
23. A. Ray, K. Rajashekara, S.N. Banavath, S.K. Pramanick, Coupled inductor-based zero current switching hybrid DC circuit breaker topologies. IEEE Trans. Ind. Appl. **55**(5), 5360–5370 (2019)
24. R. Kheirollahi, H. Zhang, S. Zhao, F. Lu, A DC SSCB based on transient current commutation. IEEE J. Emerg. Sel. Top. Power Electron. **10**, 4614–4625 (2022). https://doi.org/10.1109/JESTPE.2021.3116605

25. P. Nayak, M.V. Krishna, K. Vasudevakrishna, K. Hatua, Study of the effects of parasitic inductances and device capacitances on 1200 V, 35 A SiC MOSFET based voltage source inverter design, in 2014 IEEE International Conference on Power Electronics, Drives and Energy Systems (PEDES) (2014), pp. 1–6
26. G. Romano, A. Fayyaz, M. Riccio, L. Maresca, G. Breglio, A. Castellazzi, A. Irace, A comprehensive study of short-circuit ruggedness of silicon carbide power MOSFETs. IEEE J. Emerg. Sel. Top. Power Electron. **4**(3), 978–987 (2016)
27. R. Kheirollahi, X. Zan, S. Zhao, H. Zhang, S. Zheng, X. Lu, A-T. Avestruz, F. Lu, Capacitive couple-based transient current commutation in SSCBs. IEEE Trans. Power Electron. **37**(5), 4973–4978 (2022). https://doi.org/10.1109/TPEL.2021.3134461
28. A. A. Solangi, Y. Zhou, M. Mohammadi, R. Na, Z. J. Shen, Selective coordination of GaN-based SSCBs, in 2021 IEEE Applied Power Electronics Conference and Exposition (APEC) (2021), pp. 1140–1145, https://doi.org/10.1109/APEC42165.2021.9487323
29. R. Kheirollahi, S. Zhao, H. Zhang, X. Lu, J. Wang, F. Lu, Coordination of ultrafast SSCBs in radial DC microgrids. IEEE J. Emerg. Sel. Top. Power Electron. **10**, 4690–4702 (2022). https://doi.org/10.1109/JESTPE.2021.3109483
30. X. Zan, D. Roman, R. Kheirollahi, X. Lu, S. Zheng, F. Lu, A-T. Avestruz, Medium voltage pulse power generator for accurate current interruption. IEEE Trans. Ind. Electron. **70**, 3604–3615 (2022). https://doi.org/10.1109/TIE.2022.3174234
31. R. Kheirollahi, S. Zhao, X. Zan, H. Zhang, X. Lu, A-T. Avestruz, F. Lu, A 4kV/100A DC SSCB with soft turn-off and 99.97% efficiency, in 2022 IEEE Transportation Electrification Conference & Expo (ITEC+EATS), Anaheim, CA, June 15–17, 2022